

Award Number: W81XWH-11-1-0332

TITLE: High-Resolution Large-Field-of-View Ultrasound Breast Imager

PRINCIPAL INVESTIGATOR: Patrick LaRiviere

CONTRACTING ORGANIZATION: University of Chicago  
Chicago, IL 60637-5418

REPORT DATE: August 2014

TYPE OF REPORT: Final

PREPARED FOR: U.S. Army Medical Research and Materiel Command  
Fort Detrick, Maryland 21702-5012

DISTRIBUTION STATEMENT: Approved for Public Release;  
Distribution Unlimited

The views, opinions and/or findings contained in this report are those of the author(s) and should not be construed as an official Department of the Army position, policy or decision unless so designated by other documentation.

# REPORT DOCUMENTATION PAGE

*Form Approved*  
*OMB No. 0704-0188*

Public reporting burden for this collection of information is estimated to average 1 hour per response, including the time for reviewing instructions, searching existing data sources, gathering and maintaining the data needed, and completing and reviewing this collection of information. Send comments regarding this burden estimate or any other aspect of this collection of information, including suggestions for reducing this burden to Department of Defense, Washington Headquarters Services, Directorate for Information Operations and Reports (0704-0188), 1215 Jefferson Davis Highway, Suite 1204, Arlington, VA 22202-4302. Respondents should be aware that notwithstanding any other provision of law, no person shall be subject to any penalty for failing to comply with a collection of information if it does not display a currently valid OMB control number. **PLEASE DO NOT RETURN YOUR FORM TO THE ABOVE ADDRESS.**

<b>1. REPORT DATE</b> August 2014		<b>2. REPORT TYPE</b> Final		<b>3. DATES COVERED</b> 1 Jun 2011 – 31 May 2014	
<b>4. TITLE AND SUBTITLE</b>  High-Resolution Large-Field-of-View Ultrasound Breast Imager				<b>5a. CONTRACT NUMBER</b>	
				<b>5b. GRANT NUMBER</b> W81XWH-11-1-0332	
				<b>5c. PROGRAM ELEMENT NUMBER</b>	
<b>6. AUTHOR(S)</b>  Patrick LaRiviere  Email: pjarivi@uchicago.edu				<b>5d. PROJECT NUMBER</b>	
				<b>5e. TASK NUMBER</b>	
				<b>5f. WORK UNIT NUMBER</b>	
<b>7. PERFORMING ORGANIZATION NAME(S) AND ADDRESS(ES)</b>  University of Chicago Chicago, IL 60637-5418				<b>8. PERFORMING ORGANIZATION REPORT NUMBER</b>	
<b>9. SPONSORING / MONITORING AGENCY NAME(S) AND ADDRESS(ES)</b> U.S. Army Medical Research and Materiel Command Fort Detrick, Maryland 21702-5012				<b>10. SPONSOR/MONITOR'S ACRONYM(S)</b>	
				<b>11. SPONSOR/MONITOR'S REPORT NUMBER(S)</b>	
<b>12. DISTRIBUTION / AVAILABILITY STATEMENT</b> Approved for Public Release; Distribution Unlimited					
<b>13. SUPPLEMENTARY NOTES</b>					
<b>14. ABSTRACT</b> In this work, we sought to construct and test the first practical full-field transmission ultrasound breast imaging system. The system will ultimately have a large field-of-view capable of producing 2D images of the entire breast in near real-time. Because it uses a fixed imaging geometry that does not involve scanning, it will also circumvent the operator-dependence of conventional ultrasound imaging methods. The compact vertical design mimics the form factor of mammography systems and would provide a basis for later incorporation of an x-ray source and detector, which would allow for routine dual-modality x-ray and acoustic imaging for screening and diagnosis. The key component of the system is an acousto-optic (AO) sensor, a liquid crystal detector that converts acoustic intensity to an optically visible image. Our original design sought to use acoustic lenses to minify the acoustic image of the breast onto a small (2 inch) acousto-optic sensor, since it was then challenging to make larger AO sensors. The acoustic lenses did not produce acceptable image quality. However, a technical breakthrough allowed for production of larger AO sensors. We concluded the project by building a prototype system with a 3-inch field of view, suitable for preliminary clinical testing, and larger fields of view will be achievable in the near future.					
<b>15. SUBJECT TERMS-</b> Ultrasound, Breast cancer, Transmission ultrasound, Dense breast, Acoustography, Whole-breast ultrasound					
<b>16. SECURITY CLASSIFICATION OF:</b>			<b>17. LIMITATION OF ABSTRACT</b>	<b>18. NUMBER OF PAGES</b>	<b>19a. NAME OF RESPONSIBLE PERSON</b>
<b>a. REPORT</b> U	<b>b. ABSTRACT</b> U	<b>c. THIS PAGE</b> U			USAMRMC
			UU	25	<b>19b. TELEPHONE NUMBER</b> (include area code)

## Table of Contents

	<u>Page</u>
1. Introduction .....	4
2. Keywords .....	4
3. Overall Project Summary .....	4
4. Key Research Accomplishments.....	23
5. Conclusion.....	23
6. Publications, Abstracts, and Presentations.....	24
7. Inventions, Patents and Licenses.....	24
8. Reportable Outcomes.....	24
9. Other Achievements.....	25
10. References .....	25
11. Appendices .....	25

**Final Report for W81XWH-11-1-0332  
PI: Patrick La Riviere**

**Note: This final report builds on the previous annual reports. New sections are indicated with a marginal line.**

## **INTRODUCTION**

In this work, we are seeking to construct and test the first practical full-field transmission ultrasound breast imaging system. The system will have a large field-of-view capable of producing 2D images of the entire breast in near real-time. Because it uses a fixed imaging geometry that does not involve scanning, it will also circumvent the operator-dependence of conventional ultrasound imaging methods. The compact vertical design mimics the form factor of mammography systems and would provide a basis for later incorporation of an x-ray source and detector, which would allow for routine dual-modality x-ray and acoustic imaging for screening and diagnosis. If successful, this work will provide the basis for a dual-modality ultrasound and mammography imaging system that could help improve early detection of breast cancer, especially in young women with dense breasts, which are often not well visualized mammographically. It would also help reduce false positives, which add to the expense and anxiety associated with current approaches to breast cancer screening.

## **KEYWORDS**

Ultrasound, Breast cancer, Transmission ultrasound, Dense breast, Acoustography, Whole-breast ultrasound

## **OVERALL PROJECT SUMMARY**

**Year 1 Summary:** We made substantial progress in this first year of the project. Most tasks in the original Statement of Work for year 1 were completed on schedule. The only delay was in the optimization, fabrication, and acceptance testing of the lenses, which we had scheduled to complete within 9 months and instead wrapped up in the 13<sup>th</sup> month. This arose mainly from the need to alter our original design from a refraction-based system to a reflection-based system, due to unacceptably high levels of acoustic attenuation predicted in the refraction-based system.

**Year 2 Summary:** We fell much further behind schedule in this year due to delays in receipt of the lenses and delays involved in designing and fabricating appropriate adjustable lens mounts that allow for rotation, tilt, and translation. We were close to having a complete system by the end of year 2, which allowed for final testing in the no-cost extension period. We also explored a new direction related to using multi-frequency acquisitions to characterize lesion size.

**Year 3 Summary:** We completed assembly of the original system design, including the acoustic lenses/mirrors. Unfortunately, the obtainable image quality was extremely disappointing, with inadequate intensity and resolution and substantial distortions and artifacts. We attribute this to imperfections in the lenses interacting with nonuniformities in the acoustic field. Fortunately, our subcontractor Santec systems achieved a technical breakthrough in producing larger acoustic sensors that potentially eliminates the need for the lens system. We thus shifted our focus to the design and construction of system built around this larger-area detector that also eliminates the water bath of

previous systems. We ended the project with preliminary assembly of this new system.

**Aim 1: To design and construct a high-resolution, large field of view ultrasound breast imager by combining a super high-resolution AO sensor and a large aperture acoustic lens.**

**Task 1: Design, fabricate, and test sound source**

*1.a. Simulate acoustic propagation from array of 9 2.7" elements to confirm suitability of design choice (U of C; mos. 1-2).*

We have developed theory and software necessary to simulate the acoustic field emanating from square transducer elements. In brief, we made use of standard Rayleigh-Sommerfield diffraction theory and the angular spectrum decomposition to develop expressions for the field propagating from a rectangular piston-like transducer. By the linearity of the resulting equations, we can use superposition to determine the field produced by an array of square or rectangular transducers.

The key results are shown in Fig 1 below, which illustrates the normalized in-plane acoustic intensity distribution at a distance 2 inches from a 3" by 3" square transducer piston operating at a CW frequency of 3.35 MHz. The figure shows both a surface plot and a color mapped intensity distribution.

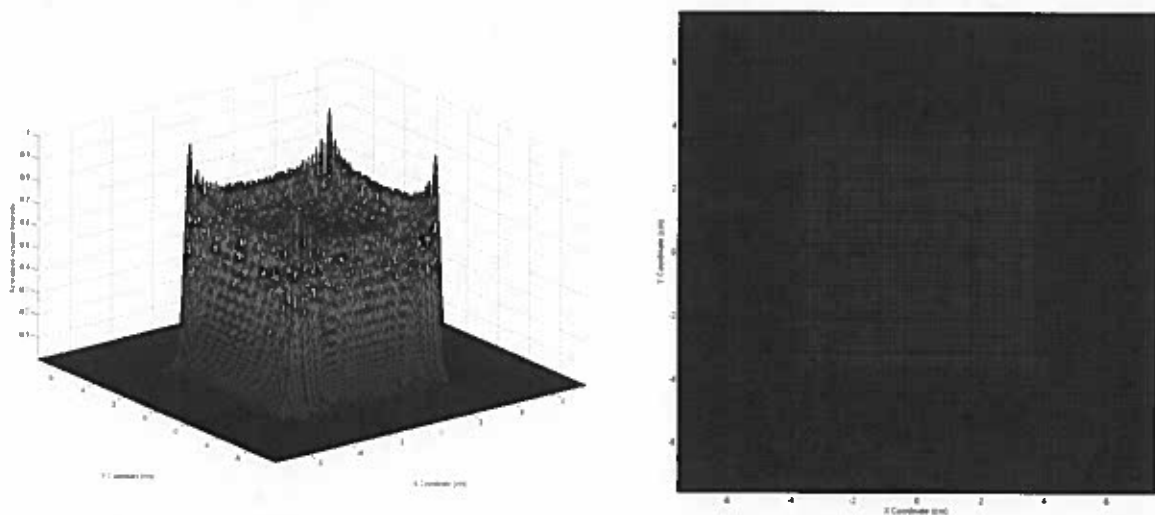


*Figure 1: (Left) The normalized in-plane acoustic intensity distribution for a 3" by 3" square transducer piston operating at a CW frequency of 3.35 MHz. The pressure field intensity is depicted in the plane parallel to the transducer surface at a distance of 2", and a background medium of water has been assumed. We note that the square modulus of the acoustic pressure field is plotted. (Right) This figure presents the same information as the left plot but shows the spatial distribution of acoustic intensity looking at the plane of interest head-on. For a planar detector positioned 2" from the transducer surface, one would expect to observe this type of diffraction pattern for an image acquired with no scattering object present.*

### 1.b. Fabricate source array (Santec; mos. 2-3)

A large-area sound source has been designed and fabricated with four 4 MHz, 3"x3" size elements. The original plan called for working at 3.35 MHz, but technical difficulties necessitated a change to 4 MHz, which should not affect any of the properties of the planned system. A quarter-wavelength acoustic matching layer was provided to allow efficient operation in water. Each element was electrically tuned to match to the 50-Ohm impedance of an RF Amplifier powered by a 4.0 MHz electrical signal from a digital function generator. An RF power splitter was also designed and built to distribute RF power equally to all 4 elements of the sound source. First-level software was also developed to allow digital control of acoustic power output of the sound source. The current design is being extended to build a larger source to cover the 8"x8" field area.

### 1.c Test source and compare with simulation results (U of C; mos. 3-4)

Comparisons indicate good agreement between the real and simulated fields.

## **Task 2: Fabricate and test AO sensor**

### 2.a Fabricate 1" X 1" AO sensor (Santec; mos. 4-5)

At least three 4 MHz AO sensors have been built. We were able to overcome some technical challenges and build even larger sensors than originally planned. The detection area of each sensor was at least 2"x2". The acoustic detection sensitivity of these sensors was found to be in the milliWatt/cm<sup>2</sup> range. The angular acceptance of the AO sensor is at least 20° about normal incidence condition. The acoustic detection sensitivity was quite dependent on the acoustic beam angle, and might impact image quality. However, this needs to be studied using the acoustic lens (or mirrors) being designed so that if needed, the AO sensor design can be change to minimize the angular effect. The milliWatt/cm<sup>2</sup> range acoustic detection sensitivity of the AO sensor should be adequate to allow us to operate the Breast Imager below the FDA specified safety standard.

### 2.b Test resolution and sensitivity of AO sensor (U of C; mos. 5-6)

We sought to characterize the spatial resolution of the prototype transmission ultrasound imaging system by deriving estimates for the edge spread function (ESF), the line spread function (LSF), and the pre-sampled modulation transfer function (MTF) of the system. We also sought to characterize the noise properties of the prototype transmission ultrasound imaging system by determining an estimate for the noise power spectrum (NPS) of the system.

#### Spatial Resolution Analysis

The spatial resolution analysis was performed using the angled edge technique originally proposed by Reichenbach *et al.* [1], in which use of a small ( $\sim 3^\circ$ ) edge angle permits finer sampling of the system ESF than the pixel pitch of a digital detector, thus minimizing the possibility of MTF aliasing. A transmission ultrasound image of a slightly angled knife edge was acquired with temporal averaging to reduce noise. A segment of the knife edge image is shown in Figure 2. Each row of pixels in Figure 2 provided a shifted sample of the knife edge. The individual rows were spatially registered by estimating the edge position within

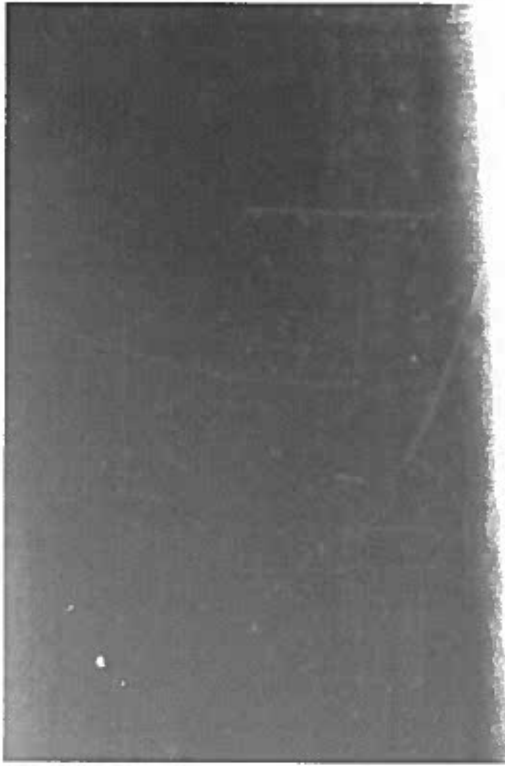


Figure 2: Image of the knife edge used to compute the pre-sampled MTF of the imaging system. The image was acquired using a peak transducer voltage of 0.7 V. Continuous frequency sweeping of 3.25-3.45 MHz at 100 MHz/s was also employed to minimize speckle artifacts due to acoustic wave coherence.

After shifting each row of pixel values by the estimated edge location, the spatially registered data points were averaged over .0625-mm intervals to obtain an estimate of the system ESF. Following the work of Boone and Seibert [2], the measured ESF data was fit to a combined error function and exponential fit of the form

$$\text{ESF}(x) = a \operatorname{sgn}(x - x_0) \{1 - \exp(-b|x - x_0|)\} + c \operatorname{erf}(\sqrt{d}(x - x_0)) + e.$$

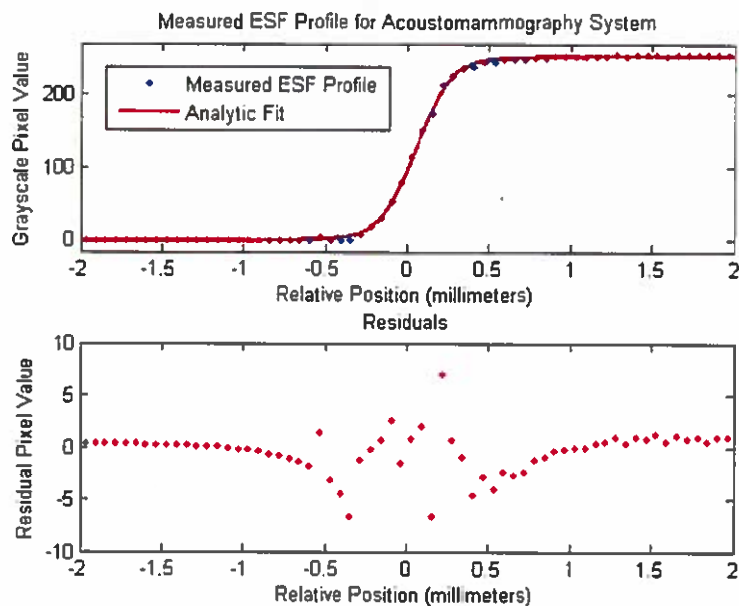
Analytic estimates for the normalized system LSF and MTF were determined from the fit parameters  $a$ ,  $b$ ,  $c$ ,  $d$ ,  $e$ , and  $x_0$  according to the relations

$$\text{LSF}(x) = \frac{1}{2(a+c)} \left[ ab \exp(-b|x - x_0|) + 2c \sqrt{\frac{d}{\pi}} \exp(-d(x - x_0)^2) \right].$$

$$\text{MTF}(f) = \frac{1}{a+c} \left[ c \exp\left(-\frac{\pi^2 f^2}{d}\right) + a \left(1 + \frac{4\pi^2 f^2}{b^2}\right)^{-1} \right].$$

### Spatial Resolution Analysis Results

Figure 3 presents the measured ESF data points with overlaid exponential-error function regression model. The statistics of the computed fit are also provided.



Regression Statistics	
Fit Coefficients:	
a	= 17.77
b	= 3.22 mm <sup>-1</sup>
c	= 108.9
d	= 17.4975 mm <sup>-2</sup>
e	= 126.3
x <sub>0</sub>	= 0.05298 mm
Goodness of fit:	
r <sup>2</sup>	= 0.9999
RMSE	= 1.426

Figure 3: Measured ESF data and analytic regression model with residual subplot. The  $r^2$  value for the regression curve is 0.9999, and the root-mean-square error (RMSE) is only 1.15% of the mean measured ESF value. These statistics indicate that the combined exponential-error function regression model provides an excellent fit to the measured data.

Figure 4 shows the normalized analytic LSF and the analytic pre-sampled MTF derived from the regression equation used to fit the ESF data in Figure 6.

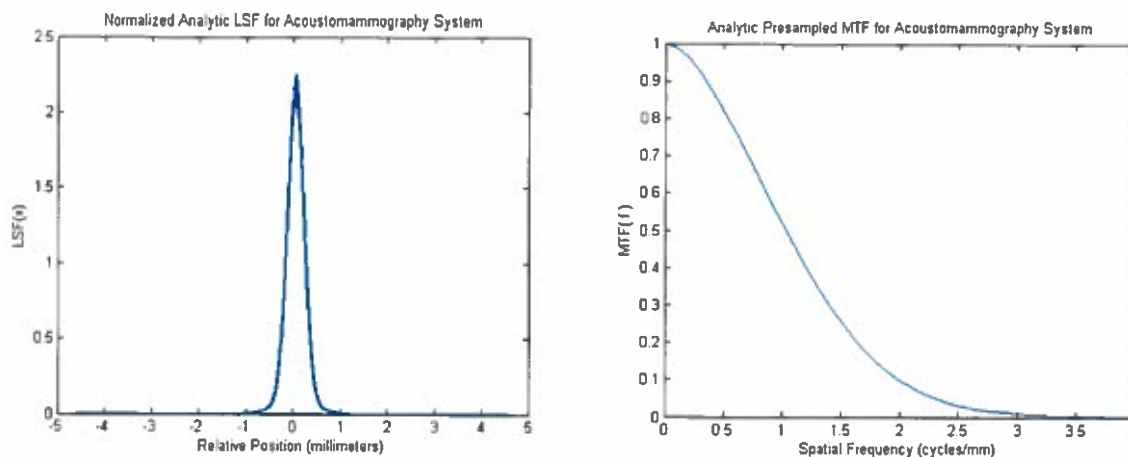


Figure 4: The normalized analytic LSF and the analytic pre-sampled MTF for the transmission ultrasound imaging system. These curves were obtained from the fitting parameters of the combined exponential-error function regression model used to fit the measured ESF data. The full-width-at-half-maximum (FWHM) of the system LSF indicates an approximate spatial resolution of 400 microns.



The FWHM of the analytic LSF was calculated to be 0.3997 millimeters, indicating an approximate spatial resolution of 400 microns for the prototype transmission ultrasound imaging system. The analytic curve for the pre-sampled MTF shows a typical Gaussian form. The curve is equal to unity at zero spatial frequency and falls off smoothly to nearly zero at the system Nyquist frequency (3.79 cycles/mm).

### Noise Analysis

The NPS of the imaging system was determined by acquiring 25 detector flood images using the same transducer settings for each acquisition. One such image is included in Figure 5. For each flood image, a subsection of the total image matrix was extracted over which the detector illumination appeared highly uniform. The NPS of each subsection was computed by subtracting the mean pixel value  $\langle PV \rangle$  and computing the square modulus of the two-dimensional discrete Fourier transform of the resulting matrix. In the continuum,

$$NPS(\mathbf{f}) = \left| \int_{-\infty-\infty}^{\infty} \int_{-\infty-\infty}^{\infty} [PV(\mathbf{r}) - \langle PV \rangle] e^{-j2\pi \mathbf{f} \cdot \mathbf{r}} d^2\mathbf{r} \right|^2.$$

The 25 separately computed noise power spectra were averaged to obtain a mean estimate for the NPS of the system. This estimate was normalized by its largest amplitude component and plotted as a two-dimensional function of spatial frequency  $\mathbf{f}$ .

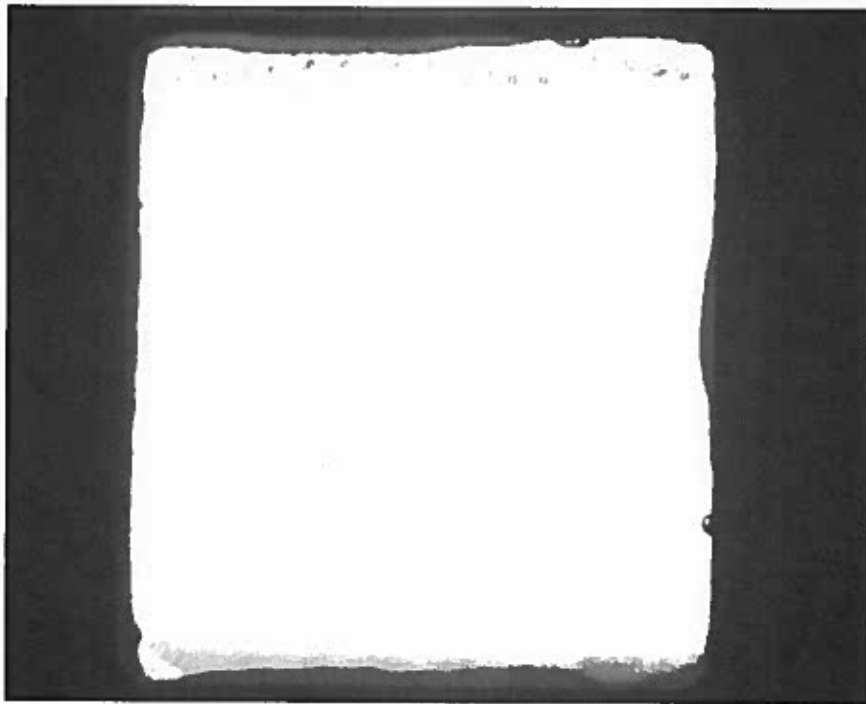


*Figure 5: Example of one of the detector flood images used to estimate the NPS of the imaging system. The image shows highly uniform illumination of the AO detector field of view. A peak transducer voltage of 2.6 V and frequency sweeping of 3.25-3.45 MHz at a rate of 100 MHz/s were used because of the uniform detector illumination provided by these settings*

Figure 6 presents an estimate of the two-dimensional NPS of the imaging system as a surface plot. The height of the NPS indicates the noise power contained per unit frequency bandwidth at each corresponding spatial frequency. It can be seen that significant noise power is contained at lower spatial

frequencies near zero frequency. The NPS amplitude falls steadily when moving toward higher spatial frequencies.

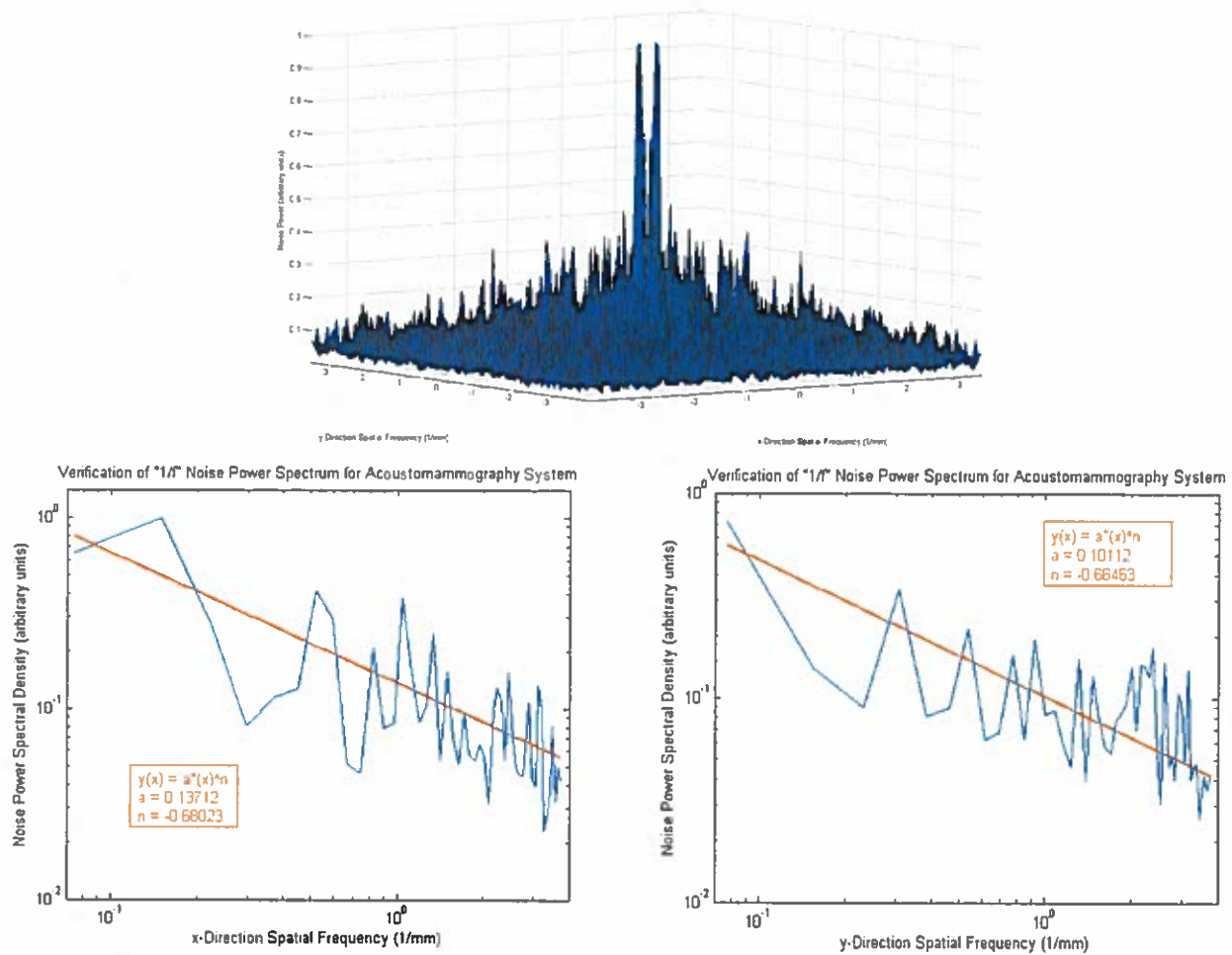


Figure 6: Surface plot of the two-dimensional NPS of the transmission ultrasound imaging system. The lower two graphs show single slices taken through the NPS surface plot along the x- and y-spatial frequency axes. These slices are plotted on log-log axes to demonstrate the presence of  $1/f$  noise in the imaging system.

The lower two plots in Figure 6 show single slices of the NPS taken along the x-spatial frequency and y-spatial frequency axes. For these graphs, the NPS is plotted on log-log axes. These slices are well fit by power law regression models, which appear as straight lines on the log-log plots. The characteristic exponent values of the regression models are  $0.680 \text{ mm}^{-1}$  and  $0.665 \text{ mm}^{-1}$  for the x- and y-directions, respectively. This type of behavior is ubiquitous in nature and is termed “ $1/f$  noise.” It is caused by random fluctuations in the solid-state circuit elements comprising most electronic devices.

#### Task conclusions

- Though the intrinsic spatial resolution of the AO detector is itself very high ( $\sim 10^{-9}$  meters) the spatial resolution of the imaging system is substantially reduced by the pixelation of the digital camera used to record the display of the AO detector for image processing and storage. The measured resolution is 400 microns.

- The noise present in the imaging system is primarily electrical in nature, as evidenced by the  $1/f$  noise behavior observed in the system NPS in both the  $x$ - and  $y$ -spatial directions.

### Multifrequency acquisition for lesion size determination

With a noise model in hand, we began to investigate a new direction involving the potential for acquiring images at two frequencies and exploiting the frequency dependence of ultrasonic attenuation to perform lesion identification and size estimation.

**Purpose:** To investigate the feasibility of using a limited number of multispectral transmission ultrasound images acquired with a novel full-field liquid crystal ultrasonic detector to estimate the sizes of cystic and malignant breast lesions.

**Methods:** In our prototype ultrasound imaging system, a high-resolution liquid crystal detector measures the intensity of the acoustic field transmitted through the compressed breast. Projection images can be acquired at multiple transducer frequencies with several monochromatic sources. Assuming normal breast parenchyma containing either a simple breast cyst or infiltrating duct carcinoma, image data acquired at two or more transducer frequencies can potentially be used to estimate the size of the lesion present. The presence of electrical Gaussian noise precludes an exact lesion thickness determination; the lesion thickness can only be estimated with some uncertainty. We have used estimation theory to derive the Cramer-Rao lower bound on the uncertainty of the thickness estimate for cystic and malignant lesions of variable sizes.

**Results:** For a 1-cm simple breast cyst and SNR of 50, an uncertainty in the estimated cyst thickness of 0.1641 cm can be obtained using two transmission ultrasound breast images acquired with transducer frequencies of 6 and 7.997 MHz. For a malignant breast lesion of the same size and SNR of 50, an uncertainty in the lesion thickness estimate of 0.197 cm can be obtained using two breast images acquired with transducer frequencies of 5 MHz and 5.462 MHz. In general, the lower bound on the precision of the thickness estimate is found to improve with increasing SNR and lesion size. Typical results are shown in Fig 7.

**Conclusion:** For the cases considered, the Cramer-Rao lower bound on the precision of the thickness estimate is significantly less than the actual lesion thickness. The precision of the thickness estimate can potentially be improved by using lower transducer frequencies, although diffraction artifacts might then become prohibitive.

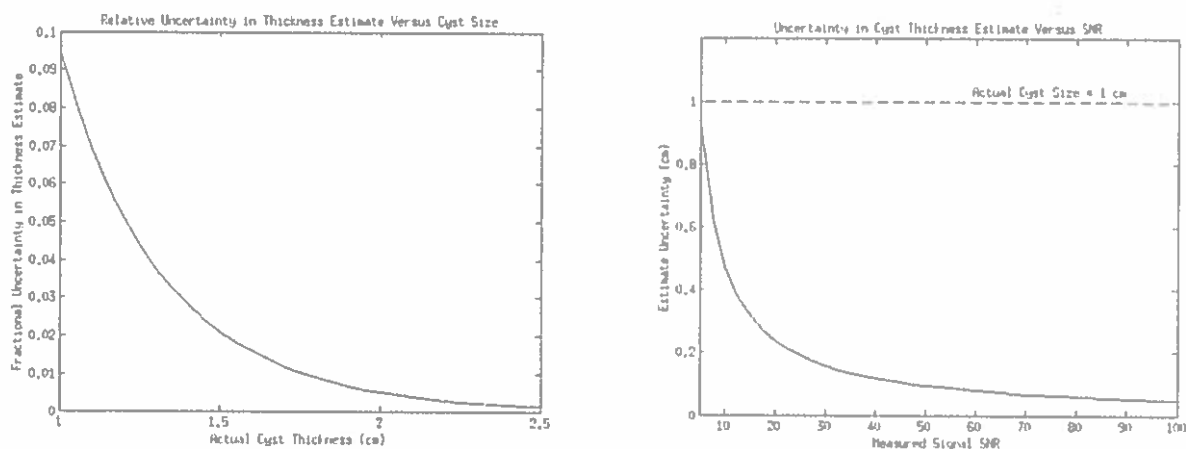


Figure 7: (Left) Relative precision of thickness estimate vs cyst size for SNR of 50. (Right) Uncertainty

*in cyst thickness estimate versus SNR.*

**Task 3: Incorporate video camera**

3.a. Incorporate the new video camera with source and AO sensor (no lens yet) and test resolution and sensitivity (U of C; mo. 6)

The video camera was incorporated both into the lens-based system and then repurposed for the large AO sensor system.

**Task 4: Design, fabricate, and test acoustic lens**

4.a. Determine final lens specifications based on simulation studies of whole system (U of C; mos 1-3)

Our initial plan was to fabricate an afocal triplet of acoustic lenses, as shown in Fig. 8.

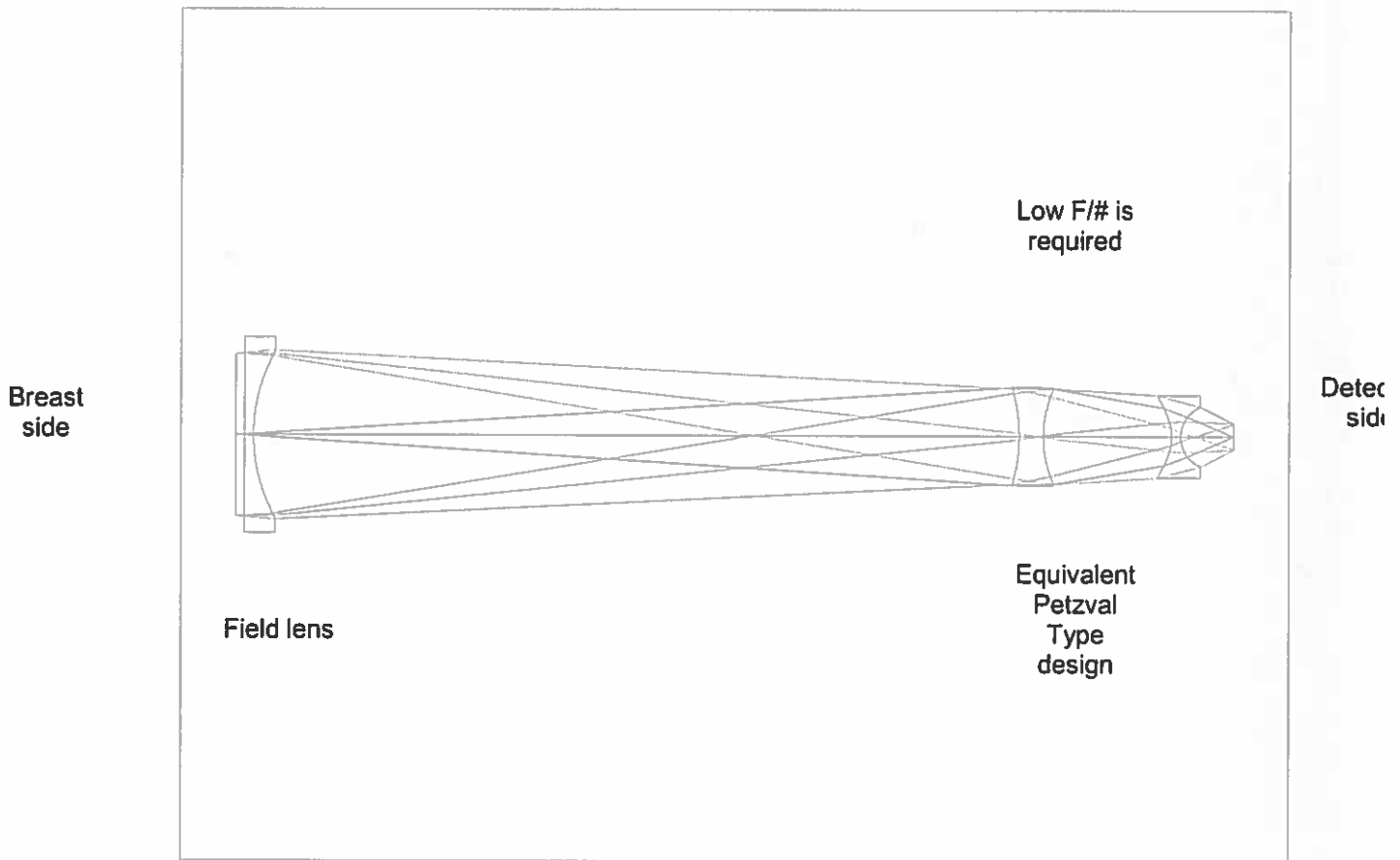


*Fig. 8: Initial afocal triplet design. The acoustic attenuation in this design would have been too high.*

However, initial design and simulation studies showed that because of the fast speed of the lens required ( $\sim F/3$  or less), the lens thickness variation would have been about  $\sim 60$  mm which would have caused unacceptable attenuation of the acoustic field.

An alternative single-lens design, shown in Fig. 8, would still have been too thick (56 mm), leading to two or three orders of magnitude of acoustic attenuation. Therefore it was decided to produce a reflective system rather than a refractive lens.

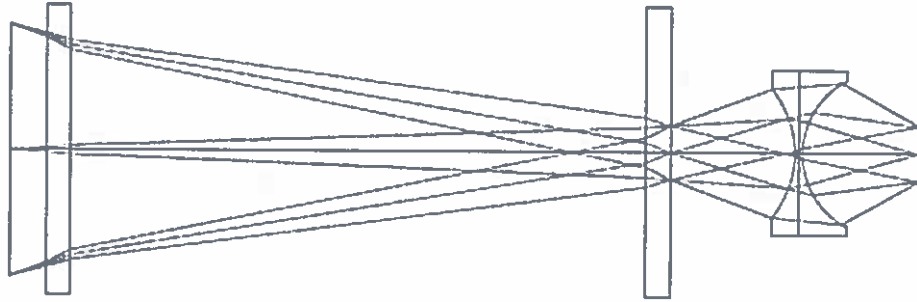


*Fig 9: A single-lens design aimed at reducing acoustic attenuation still would have had unacceptable levels of it. We turned instead to a reflection-based system.*

4.b. Optimize lens design using Zemax lens design software (U of C/Sasian; mos. 4-6)

We used the Zemax lens design software to optimize the mirror-based system. The schematic of the optimized mirror-based system is shown below in Fig 10

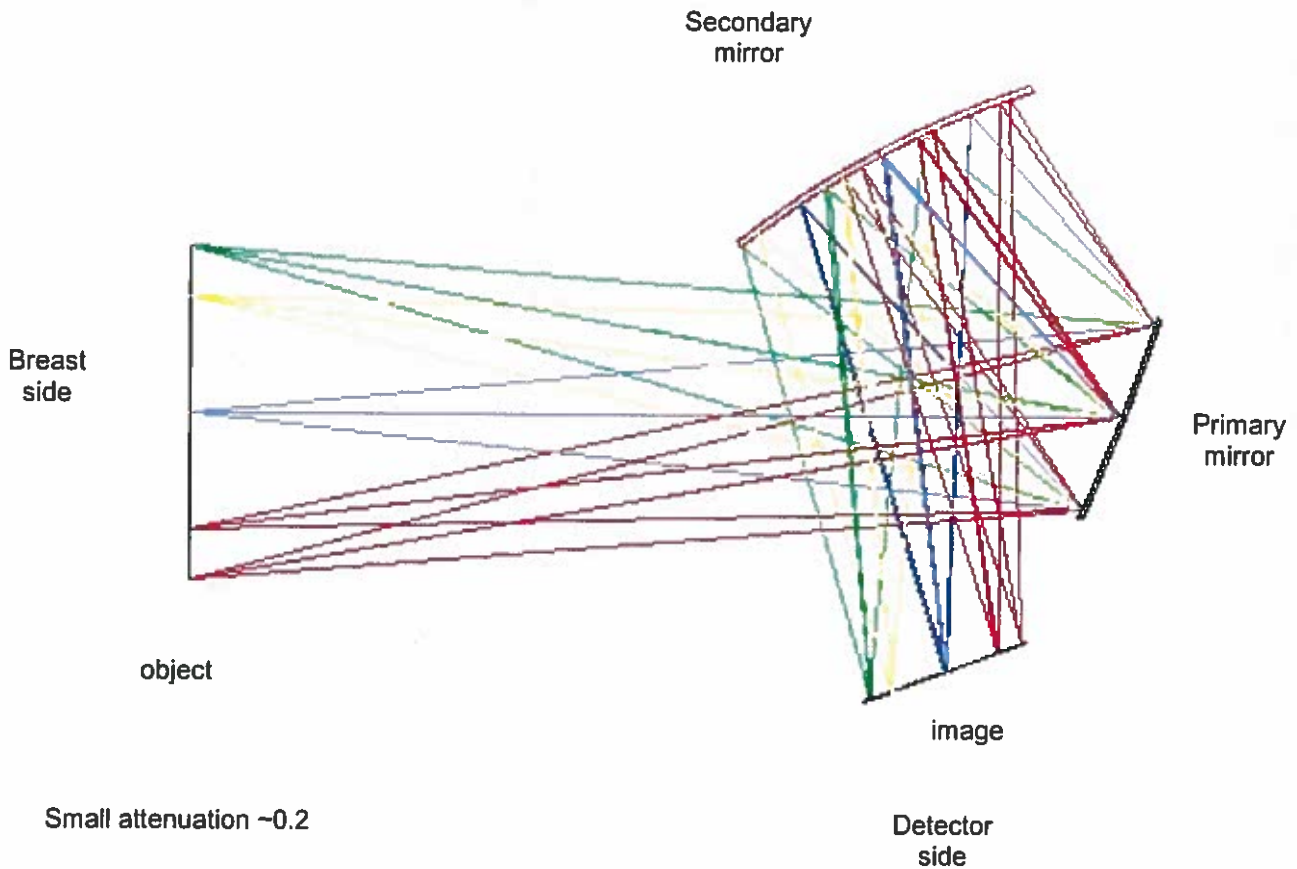


*Fig 10: Cross-sectional schematic of the lens-based system.*

A three-dimensional rendering is shown in Fig. 11.



*Fig 11: Three-dimensional view of the mirror-based system.*

The system characteristics are as follows:

- Length: 600 mm
- Width: 310 mm
- Working F/# = 2.88
- Wavelength: 0.5 mm
- Stop aperture at primary mirror
- Other apertures for stray sound suppression are allowed
- System is plane symmetric in y-z plane
- Magnification 0.5

The primary mirror surface, which is concave, is described by

$$sag = \frac{c(x^2 + y^2)}{1 + \sqrt{1 - c^2(x^2 + y^2)}} + Ay^2 + Bx^2y + Cy^3$$

with parameters

- $c = -1/1000$  mm
- $A = 1.555861e-4$  mm<sup>-1</sup>
- $B = 5.74993e-7$  mm<sup>-2</sup>
- $C = 5.160419e-7$  mm<sup>-2</sup>
- Diameter = 130 mm

With these specifications, the expected performance is given in the Airy disk diagrams shown in Fig. 12.

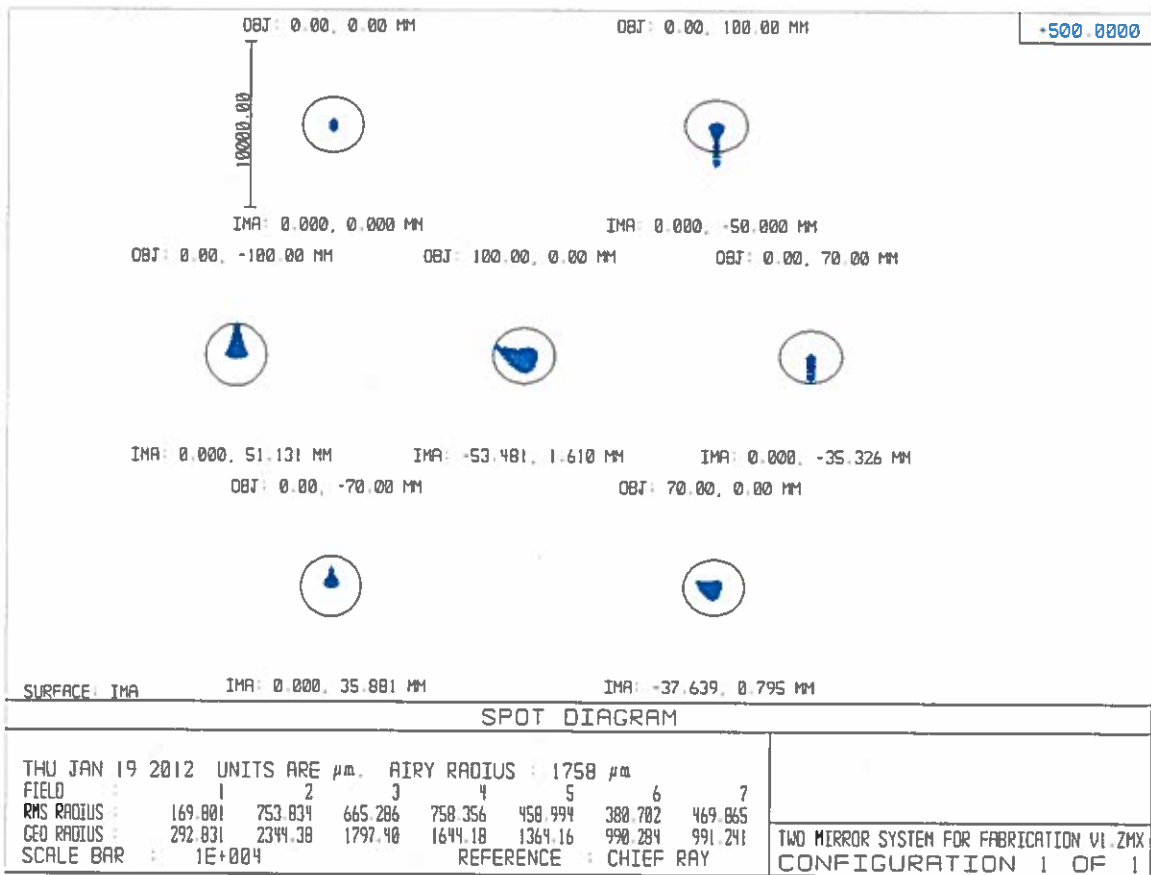


Fig 12: Airy spot diagrams showing expected performance of the lens system.

4.c. Fabricate lens (U of C/Sasian; mos. 7-8)

The lenses were successfully fabricated by Lam Optics in Tucson, AZ.

4.d. Perform acceptance testing on lens (U of C; mo. 9)

Consultant Jose Sasian personally visited the fabrication facility to observe fabrication and oversaw in-house quality assurance. He performed preliminary acceptance testing before the lenses were sent to the University of Chicago. Final testing will take place during alignment and focusing.

**Task 5: Assemble complete system**

5.a. Fabricate immersion tank (Santec; mo. 9)

An appropriate immersion tank was assembled by Santec systems Inc.

5.b. Assemble system (U of C; mo. 10-12)

Assembly of the complete system was delayed by late delivery of the lenses and further slowed by delays in fabricating appropriate adjustable mounts for the acoustic mirrors. Any sort of compound focusing system requires careful positioning and alignment. For optical lenses and mirrors, there are many vendors providing off-the-shelf mounts that allow for fine adjustment and stable positioning. Such mounts are not readily available for the kind of large acoustic mirrors we ended up designing for this

project. Thus for our problem we need a customized solution. The spacings and rotation and tilt angles are given in Fig. 13.

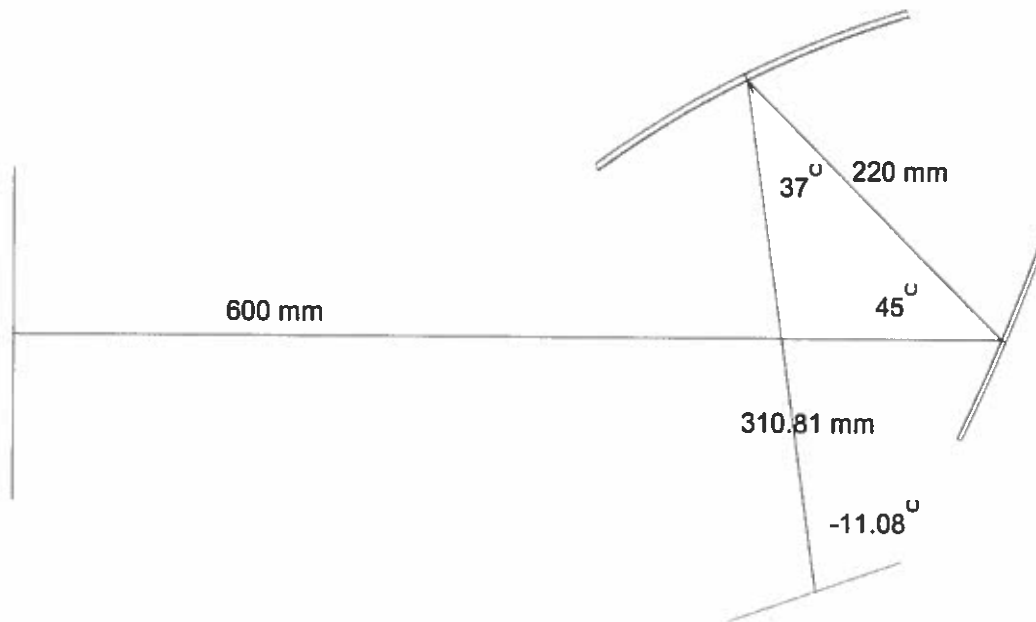


*Fig 13: Mirror spacings and angles.*

We determined the following specifications for the lens mounts:

**Primary mirror:**

- Needs to be able to tilt in X and Y ~8 degrees
- Needs to be able to be located in XYZ by ~+/- 5 mm
- Needs to be able to rotate ~+/- 12 degrees
- Select three point mount
- Attach support to mirror back
- Use mirror with toroid and comatic shape

**Secondary mirror:**

- Needs to be able to tilt in X and Y ~8 degrees
- Needs to be able to be located in XYZ by ~+/- 5 mm
- Select three point mount
- Attach support to mirror back

**Sensor:**

- Needs to be able to tilt in X and Y ~8 degrees
- Needs to be able to be located in XYZ by ~+/- 5 mm



Suitable mounts have been designed and fabricated and alignment is currently underway using a laser to align mirrors to proper distances, followed by a point source allowing for final alignment as shown in Figs. 14 and 15.

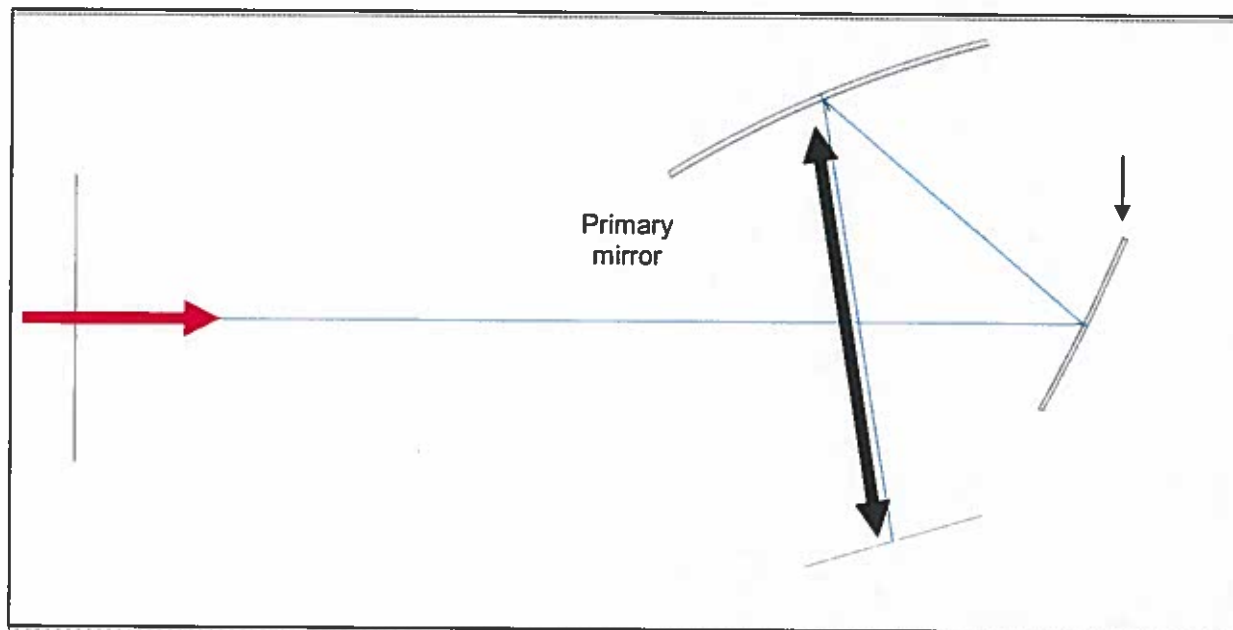


*Fig 14: Preliminary alignment strategy*

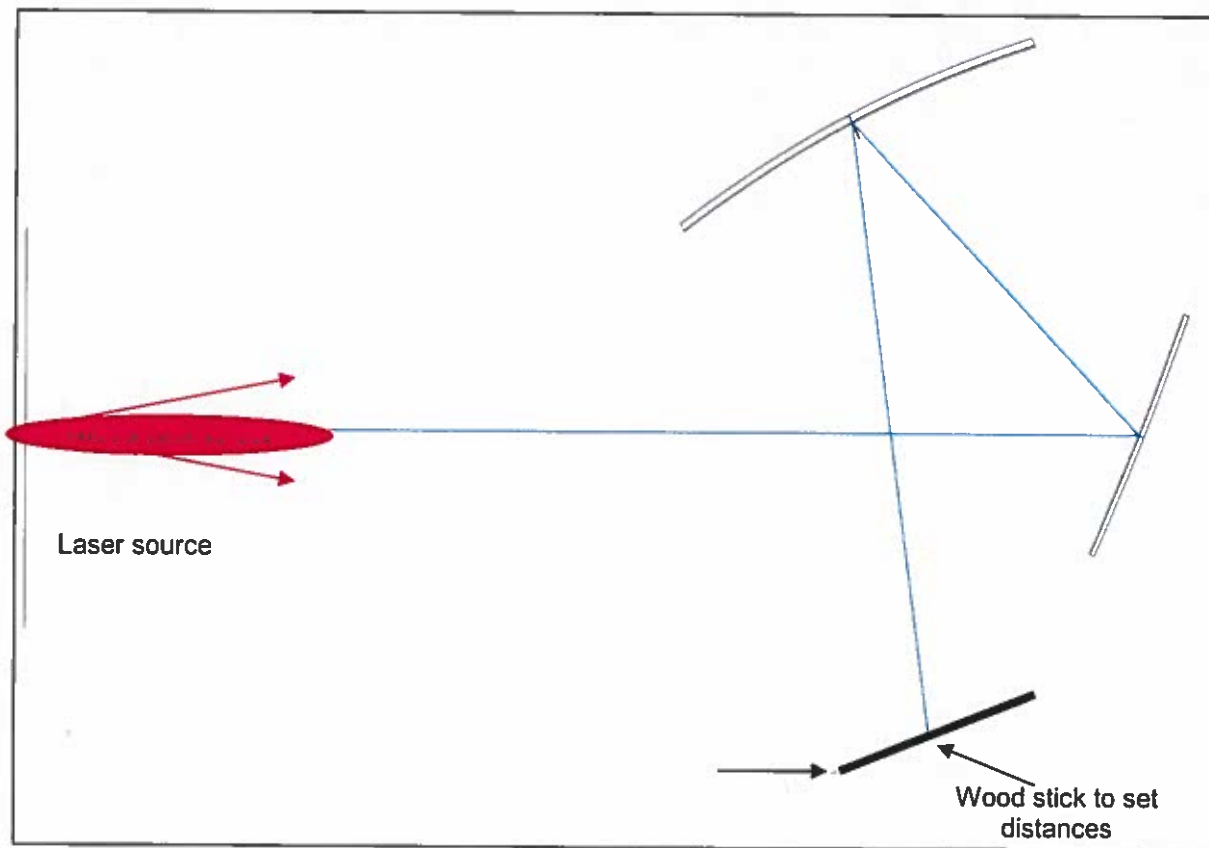


*Fig 15: Final alignment strategy*

**Aim 2: To use breast phantoms to test feasibility and performance of the high-resolution, large field of view ultrasound breast imager**

**Task 6: Perform resolution, noise contrast studies**

We characterized the contrast response of the AO sensor as a function of varying exposure time and applied voltage. The results are shown in Fig. 16.

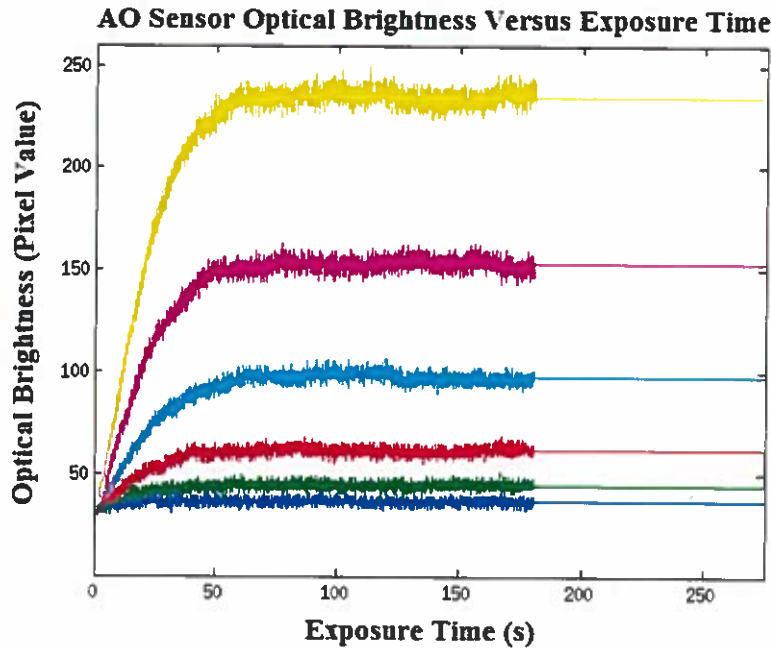


Figure 16: Response of AO sensor as a function of exposure time for varying voltages.

We found that the response was well described by the following bi-exponential

$$B(t) = B_{min} + B_0 \sin^2 \left\{ \delta_{fast} \left[ 1 - \exp(-t / \tau_{fast}) \right]^2 + \delta_{slow} \left[ 1 - \exp(-t / \tau_{slow}) \right]^2 \right\}$$

We were then able to use these results to generate the steady-state acousto-optic transfer curve:

$$B(\mathbf{r}) = T(I(\mathbf{r}))$$

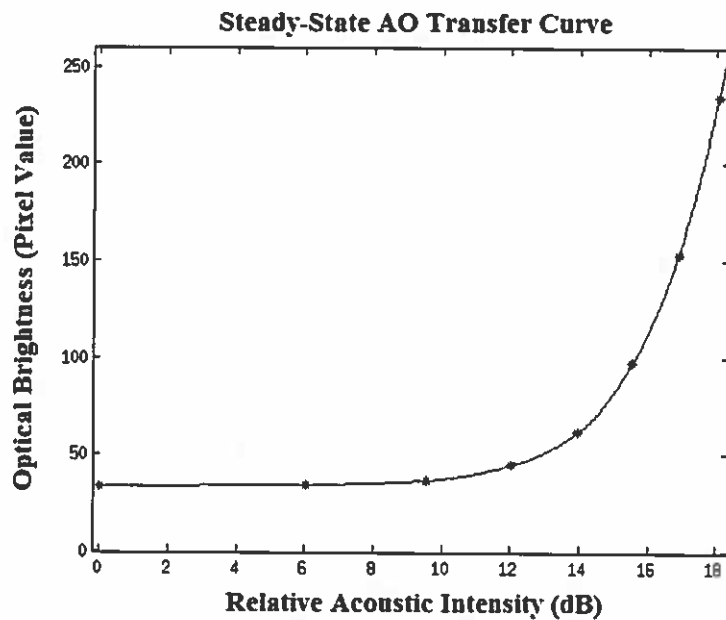


Fig 17: Transfer curve of the AO sensor.

Using these findings, we were able to perform lesion detectability studies using the K wave simulation package [3]. We simulated a dense breast (75% parenchyma and 25% fat) and lesions of diameter 1, 0.5, and 0.25 cm. The boundary between subcutaneous fat and parenchymal tissue was given a jagged interface in order to produce realistic levels of scattered background structure in the resulting images.

**Dense Breast Phantom (75% parenchyma, 25% fat)**

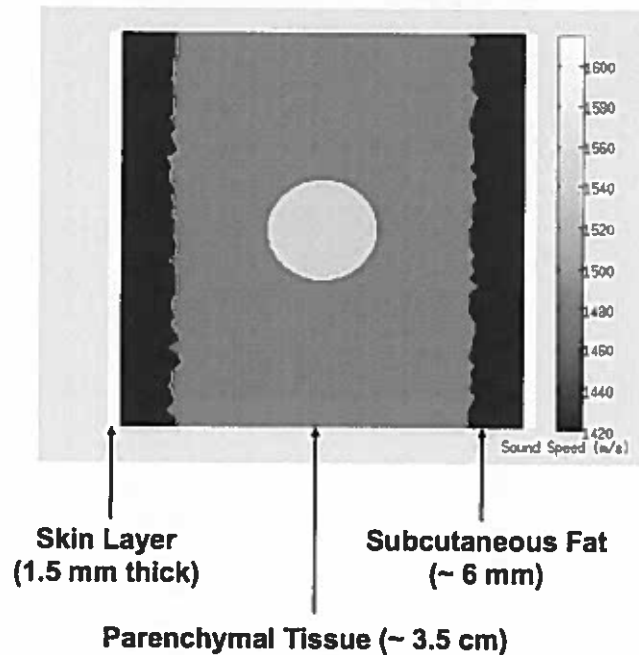
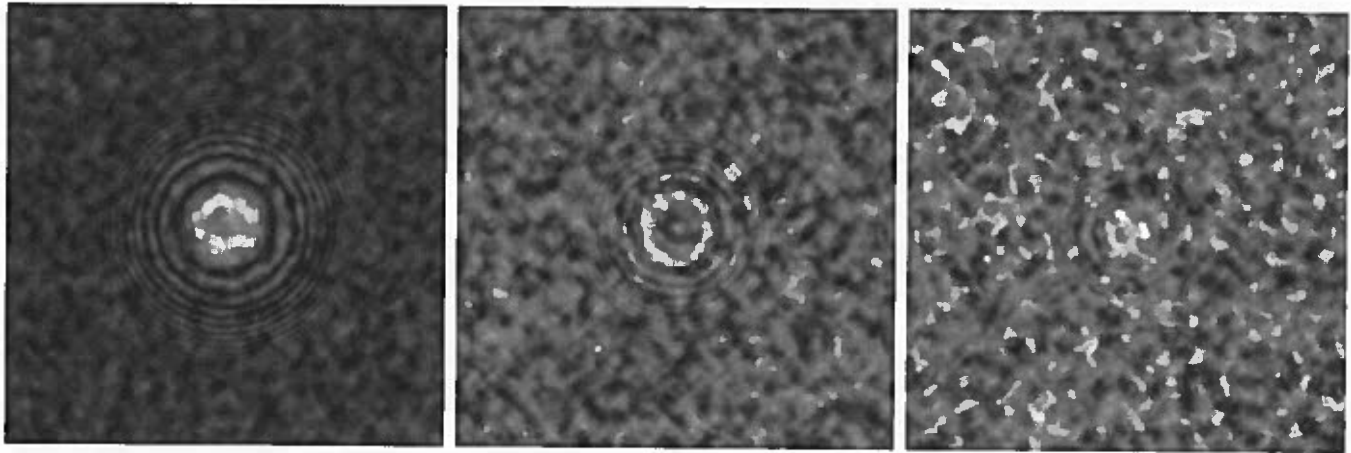


Figure 18: Numerical phantom used for simulation.



1 cm

0.5 cm

0.25 cm

*Figure 19: Simulation results for lesions of diameter 1 cm, 0.5 cm, and 0.25 cm.*

#### **Task 7: Perform phantom measurements**

The original lens-based system failed to yield images that were even worthy of systematic characterization. We attribute this to imperfections in the lenses interacting with nonuniformities in the acoustic field. Fortunately, our subcontractor Santec systems achieved a technical breakthrough in producing larger acoustic sensors that potentially eliminates the need for the lens system. We thus shifted our focus to the design and construction of system built around this larger area detector that also eliminates the water bath of previous systems.

#### **Task 8: Refine and adjust system**

8.a. Refine and adjust system in response to phantom experiments (U of C and Santec; mos. 19-24)

The new system design is shown in Fig. 20. A photograph of the system is shown in Fig. 21.

The system design specifications are listed in Table 1. We are currently tuning the final electronics and image acquisition optics. The system should be ready for phantom testing in a few weeks and hopefully for clinical testing within a few months.

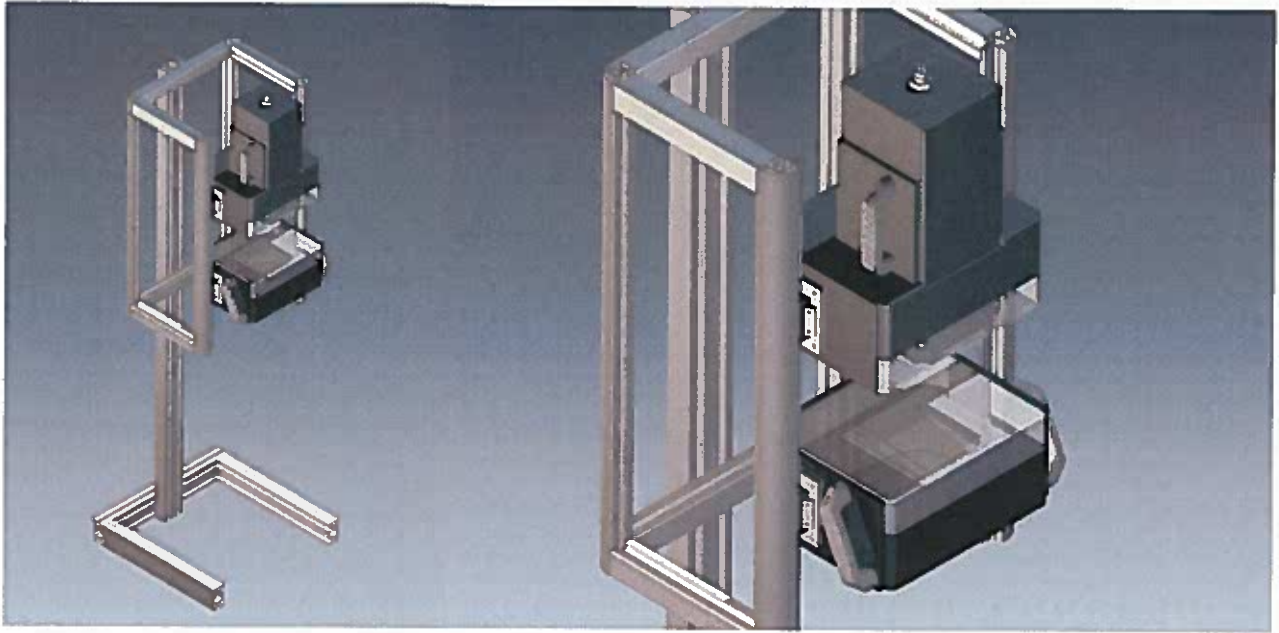


*Figure 20: Schematics of new large-area system.*

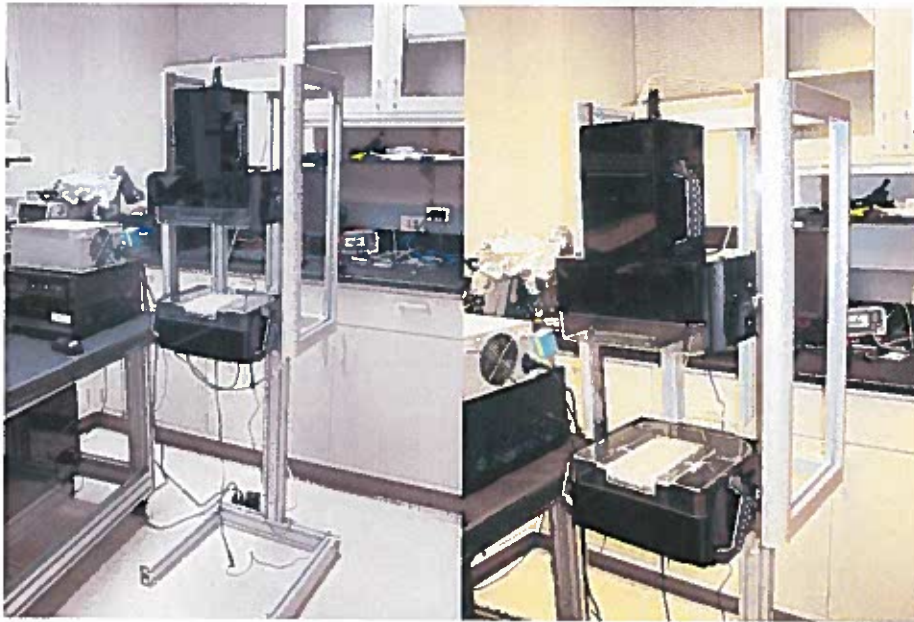


*Figure 21: Photographs of new large-area system.*

**TABLE 1: SYSTEM SPECIFICATIONS**

**AO IMAGING UNIT:**

**AO-Sensor:**

- Field of View: 3.15 in. x 3.15in.
- Operating Frequency: 3.8 MHz +/- 0.5 MHz
- Sound Detection Threshold: 1-5 mW/cm<sup>2</sup>
- Image Erasure Unit: 1kHz, <10V<sub>pp</sub>

**Viewing Optics for Acousto-Optic Detector:**

- Precision Polarization Light Box: ≥3.15 in. x 3.15 in.
- Digital Video Camera: Resolution: 659x494, Sensor: ½" CCD Sony ICX4. Max Frame Rate: 50 fps
- Color: Monochromatic
- Interface: 1394 Firewire bus
- Lens Mount: C-Mount

**SOUND SOURCE:**

**Sound Source:**

- Sound Radiating Area: 3.15 in. x 3.15 in.
- Operating Frequency: 3.8 MHz +/- 0.5 MHz
- Acoustic Power Output: >0.5 W/cm<sup>2</sup>

**Drive Electronics :**

- Signal Source Function Generator: DC to 10 MHz, Frequency Resolution: 48 bits Channel 2  
Amplitude: ±10V; Output Impedance: 50Ω
- RF Amplifier:
  - Frequency:10kHz to 6MHz
  - Gain: 52dB±1dB
  - RF Power Input Drive: 0dB (1mW) typical
  - RF Power Output Power: >100 W
  - Reflected Power Protection: 150W max.
  - Input & Output Impedance: 50Ω
  - Operating Temperature: 0°C to 40°C
  - AC Input: 180 to 264VAC, 47 to 63 Hz @5A
  - Circuit Protection: Internally fused at internal power

## KEY RESEARCH ACCOMPLISHMENTS

- Successful simulation and construction of acoustic field of multielement sound source.
- Successful construction of 2-inch acousto optic (AO) sensor.
- Measurement of noise and spatial resolution properties of AO sensor coupled with existing video camera.
- Development and characterization of multiple acoustic lens systems, resulting in a very original acoustic-mirror design that should minimize acoustic attenuation relative to the original refraction-based designs.
- Analysis of potential for multi-frequency acquisition technique to determine lesion type and size.
- Fabrication of lenses.
- Fabrication of tank.
- Design of lens mounts and focusing system.
- Assembly and testing of complete system.
- Successful construction of 3-inch acousto optic (AO) sensor.
- Redesign of vertical system without water bath
- Detectability analysis
- Preliminary system assembly

## CONCLUSION

Year 1: We made excellent progress through year 1. The simulation and construction of the sound sources and AO sensors went according to schedule and careful measurements showed that the system resolution of the AO sensor coupled with the current video sensor is ~400 microns. The noise present in the imaging system is primarily electrical in nature, as evidenced by the  $1/f$  noise behavior observed in the system NPS in both the  $x$ - and  $y$ -spatial directions. Our initial lens design proved impractical because of the large acoustic attenuation of the materials needed to achieve the design, but we produced a strong alternative design based on the use of acoustic mirrors.

Year 2: We fell much further behind schedule this year due to delays in receipt of the lenses and delays involved in designing and fabricating appropriate adjustable mounts that allow for rotation, tilt, and translation. We are very close to having a complete system that will allow for final testing in the no-cost extension period. We also explored a new direction related to using multi-frequency acquisitions to characterize lesion size.

Year 3: We concluded that the initial design involving a small AO sensor and lenses was not likely to succeed. The field of acoustical lenses is not as mature as that of optical lenses, and the combination of lens imperfections and source inhomogeneities led to unacceptable image quality. However, the technical barriers to developing larger AO sensors have been overcome, so we have developed a promising prototype around a 3 inch X 3 inch sensor, with the potential for scaling to larger sizes in the near future.

### PUBLICATIONS, ABSTRACTS, AND PRESENTATIONS

- Poster presentation: *J.R. Rosenfield, J.S. Sandhu, J.K. Tawiah, and P.J. La Rivière*, "Evaluation of the Spatial Resolution and Noise Properties of a Prototype Transmission Ultrasound Breast Imaging System Employing an Acousto-Optic Detector," NIH NIBIB training grant symposium, June, 2012.
- Oral presentation: *J.R. Rosenfield, J.S. Sandhu, J.K. Tawiah, and P.J. La Rivière*, "Evaluation of the Spatial Resolution and Noise Properties of a Prototype Transmission Ultrasound Imaging System Employing An Acousto-Optic (AO) Detector," AAPM Annual Meeting, July, 2012.
- Oral presentation, *J.R. Rosenfield, J.S. Sandhu, and P.J. La Rivière*, "Using Monochromatic Sources to Obtain Depth Information in Multispectral Transmission Ultrasound Breast Imaging," AAPM Annual Meeting, August, 2013.
- Oral presentation: *J.R. Rosenfield, J.S. Sandhu, and P.J. La Rivière*, "An Investigation of the Dynamic Response of a Novel Acousto-Optic Liquid Crystal Detector for Full-Field Transmission Ultrasound Breast Imaging," *AAPM annual meeting, 2014 (Student paper competition finalist)*.
- Oral presentation: *J.R. Rosenfield, J.S. Sandhu, and P.J. La Rivière*, "Receiver operating characteristic analysis for the detectability of malignant breast lesions in acousto-optic transmission ultrasound breast imaging," Acoustical Society of America, 2014.

### INVENTIONS, PATENTS AND LICENSES

Nothing to report.

### REPORTABLE OUTCOMES

The research has led to the development of a prototype transmission ultrasound system in a vertical, mammography-like configuration. After further phantom testing, it will be ready for patient testing.



## OTHER ACHIEVEMENTS

### *List of supported personnel:*

1. Patrick La Riviere, Ph.D., Associate Professor of Radiology, The University of Chicago
2. Hiroyuki Abe, MD, Ph.D., Associate Professor of Radiology, The University of Chicago
3. Jonathan Rosenfield, M.S., M.M.P., Graduate Research Assistant, Committee on Medical Physics, The University of Chicago

## REFERENCES

- [1] S. E. Reichenbach, S. K. Park, and R. Narayanswamy, "Characterizing digital image acquisition devices," *Opt. Eng. (Bellingham)* **30**, 170–177 (1991).
- [2] J.M. Boone and J. A. Seibert, "An analytical edge spread function model for computer fitting and subsequent calculation of the LSF and MTF," *Med Phys.* **21**, 1541-1545 (1994).

## APPENDICES

Not applicable.